Sustainable Energy Technologies and Assessments 43 (2021) 100897

Contents lists available at ScienceDirect

Sustainable Energy Technologies and Assessments

journal homepage: www.elsevier.com/locate/seta

Original article

Impact of the reverse water-gas shift operating conditions on the Power-to-Liquid process efficiency

Sandra Adelung *, Simon Maier, Ralph-Uwe Dietrich

German Aerospace Center (DLR), Pfaffenwaldring 38-40, 70569 Stuttgart, Germany

ARTICLE INFO

Keywords:
Synthetic fuels
Alternative fuels
rWGS
Syngas
Syncrude

ABSTRACT

Fischer-Tropsch based fuels from renewable electricity and carbon dioxide provide one possibility to defossilise the transport sector, especially where long distances and high loads require fuels with high energy density. In this work, a stationary Power-to-Liquid (PtL) process model is set up in Aspen Plus®. The process involves CO_2 absorption, water electrolysis, CO_2 activation by reverse water-gas shift reaction (rWGS), an oxyfuel burner, Fischer-Tropsch synthesis, product separation and hydrocracking. The influence of the rWGS operating conditions (pressure and temperature) on the overall process performance in terms of PtL-efficiency and hydrogen/carbon efficiency is investigated. The operating conditions are varied between 550 and 950 °C and 1–25 bar. The temperature and pressure dependent methane formation in the rWGS is found to have major influence on the efficiencies. For the base case, a maximum Power-to-Liquid efficiency of $\eta_{PtL} = 38.7$ % is obtained at 5 bar and 825 °C, while a maximum hydrogen efficiency of $\eta_H = 28$ % results at 1 bar and 725 °C. The carbon efficiency is found to be constant ($\eta_C = 88$ %). Sensitivity studies show that the optimum operating conditions are not affected significantly by variation of the investigated process variables.

Introduction

Motivation for Power-to-Liquid

In order to limit the temperature increase to 1.5 °C, in comparison to 1990 [1], global actions in all energy sectors have to be taken to reduce greenhouse gas emissions (GHG). One crucial contributor is the transport sector, where global direct emissions reached 7 Gt of CO_2 equivalents ($CO_{2,eq}$) in 2010 [2]. This correlates to 23 % of the total energy related emissions [2]. Decarbonizing the transport sector poses a challenge regarding the difficult-to-electrify sectors (marine, heavy-duty vehicles, aviation), where high energy densities are required. In 2010, aviation accounted for 10.6 % of the GHG emissions of the transport sector, which equals 743 Mt $CO_{2,eq}$ [2]. In 2016 the civil aviation sector emitted 814 Mt CO_2, which is about 2 % of the anthropogenic carbon emissions [3]. Without further action the carbon dioxide emissions are expected to increase due to passenger growth [4,5]. In 2009, to reduce GHG emissions in the aviation sector, the International Air Transport Association (IATA) set itself three main goals [5]:

- 1.5 % increase of fuel efficiency p.a. from 2010 until 2020,
- Carbon-neutral growth starting 2020,
- 50 % reduction of net-CO_2 emissions until 2050, compared to 2005.

In 2017, the IATA reported that the first goal was, until then, "surpassed" [6]. In 2019, the IATA states they are "on track" to reach the first goal [3]. The IATA expects that, especially for long-haul aircrafts, liquid fuels will be required at least for the next 50 years [7]. Hence, to reach the latter two goals, large amounts of Sustainable Alternative Fuels (SAF) will be required [7]. Besides biomass-based fuel production routes, synthetic hydrocarbons can be obtained from renewable electricity (e.g. from wind and solar power) in a Power-to-Liquid (PtL) process [4]. According to the International Civil Air Transport Association (ICAO), the PtL process via Fischer-Tropsch (FT) synthesis should be considered as a measure to reduce GHG emissions [4]. Since 2009, FT synthesized isoparaffinic kerosene (FT-SPK) can be added with up to 50% as drop-in jet fuel [4]. For PtL jet fuel Schmidt *et al.* estimate a reduction of 70 % to > 95 % of specific GHG emissions in comparison to conventional jet fuel [8].

* Corresponding author.
E-mail addresses: Sandra.Adelung@dlr.de (S. Adelung), Simon.Maier@dlr.de (S. Maier), Ralph-Uwe.Dietrich@dlr.de (R.-U. Dietrich).

https://doi.org/10.1016/j.seta.2020.100897
Received 27 July 2020; Received in revised form 12 October 2020; Accepted 25 October 2020
Available online 13 November 2020

Basic process description

The production of liquid fuels from renewable electricity has been previously studied e.g. by [8–15], who investigated different process designs for example different strategies for using the tail gas, different hydrogen and carbon monoxide production routes and different FT reactors. [13,15] have studied similar PtL process configurations as described in this work. Vázquez *et al.* give insight on the performance of their PtL bench-scale plant SOLETAIR and state the operating conditions of each unit [15]. They analyze the process for further improvement in a theoretical study [15]. The pilot plant has a hydrogen efficiency (based on the overall FT products) of 30.8 % and a carbon efficiency of 59.5 % [15]. König *et al.* set up a PtL process model and evaluate the process for a fixed set of unit assumptions [13]. They calculate a PtL-efficiency of 43.3 % and a carbon efficiency of 73.7 % [13]. In comparison, the pilot plant lacks utilization/recycling of the tail gas, which probably explains the higher carbon efficiency in [13].

Fig. 1 shows one possible process configuration to produce synthetic hydrocarbons from renewable electricity. Carbon dioxide can be recovered from different point sources like steel factories, cement plants, power plants, or via direct air capture. As water and CO_2 are very stable molecules, the production of more reactive hydrogen and carbon monoxide requires a significant amount of energy. In the depicted approach, first the liquid water is split to form hydrogen via electrolysis (i) and second the CO_2 is activated to form CO in a reverse water-gas shift reaction (ii). The heat for the rWGS unit is provided by burning gaseous products from the product separation. In addition to the rWGS reaction itself, different side reactions may occur in the rWGS unit (see 1.3).

$$H_2O_{(l)} \rightarrow H_2 + 0.5\ O_2 \quad \Delta_R H^0 = 285\ \mathrm{kJ/mol} \tag{i}$$

$$CO_2 + H_2 \rightleftharpoons CO + H_2O_{(g)} \quad \Delta_R H^0 = 41\ \mathrm{kJ/mol} \tag{ii}$$

$$CO + 2\ H_2 \rightarrow (-CH_2-) + H_2O_{(g)} \quad \Delta_R H^0 = -152\ \mathrm{kJ/mol} \tag{iii}$$

The syngas is further converted in the exothermic FT reaction (iii) into a broad range of hydrocarbons. Long chained hydrocarbons are cracked in a hydrocracker to increase the output of the desired chain length for fuel production ($<C_{22}$). Gaseous products and unreacted educts are recycled to increase the carbon efficiency of the process (further information on the recycles see chapter 2).

To maximize the energetic efficiency, matching rWGS and FTS process parameters are required in order to maximize the production of desired liquid fuel, by minimizing side reactions and reusing unavoidable by-products. Optimal process parameters cannot be found on a unit-by-unit optimization basis, but only by adjusting all parameters of the entire PtL process simultaneously. Additionally, the selection of different technologies might lead to different optimum rWGS operating conditions. The Fischer-Tropsch synthesis can, for example, be conducted in a slurry reactor or a fixed bed reactor with different kinds of catalysts and at different operating conditions, e.g. temperatures (high and low temperature FTS) [16]. This will affect the FTS boundary conditions (required feed composition in terms of H_2/CO ratio and inert gas content) as well as the performance of the FTS (CO conversion and hydrocarbon product distribution). Hence, different FT reactor types may influence the stream properties in the PtL process significantly. Consequently, different FT reactor types may lead to a different set of optimum rWGS operation conditions.

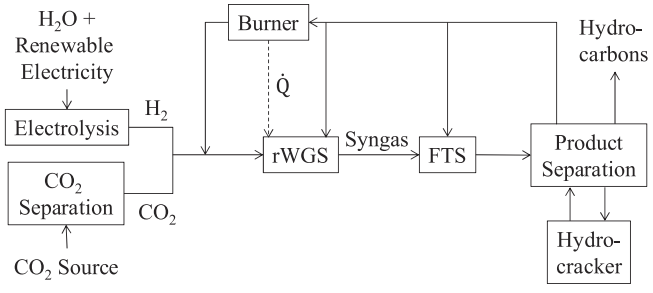

Fig. 1. Basic process scheme of the Power-to-Liquid process via Fischer-Tropsch synthesis (FTS) and reverse water-gas shift reaction (rWGS), including recycles to increase the carbon efficiency.

Different rWGS operating conditions have been applied in the literature. [13] and [15] have studied similar PtL process configurations as described in this work. König *et al.* assume $T_{rWGS} = 900\ ^\circ C$ and $p_{rWGS} = 25$ bar ($p_{FTS} = 25$ bar) in their process model [13]. Vázquez *et al.* operate their pilot plant at 850 °C and 1–5 bar [15]. However, they expect an improvement of energetic efficiency, if the rWGS reactor is operated at FT pressure level ($p_{FTS} = 20$–30 bar) [15]. A comparison of the energy efficiencies in [13] and [15] does not bring clarification which operating conditions are superior as they are additionally affected by other varying assumptions. To compare different rWGS operating conditions, constant boundary conditions, process unit assumptions and process configuration assumptions are required. To the author's knowledge, no systematic studies have been published on the influence of different rWGS operating conditions on the overall Power-to-Liquid process efficiency.

Syngas production – thermodynamics

The task of the rWGS unit is to produce carbon monoxide for the subsequent FT synthesis. The rWGS operating conditions affect the tail gas recycle and consequently the rWGS feed (compare Fig. 1). In addition to the rWGS reaction (ii), reactions involving methane and carbon may occur in the syngas reactor. Methane is formed in the FT reactor and can be formed or reformed in the rWGS unit depending on the rWGS operating conditions and the rWGS feed composition. The methane reforming reactions (iv)-(vi) are endothermic and thus methane reforming is thermodynamically favored at higher temperatures [17]. From the stoichiometry of reaction (iv)-(vi) follows that decreasing the pressure shifts the equilibrium to the right side and thus leads to lower a methane concentration in the product. Hence, to maximize the CO formation in the rWGS reactor, low pressures and high temperatures are required.

$$CH_4 + H_2O \rightleftharpoons 3\ H_2 + CO \quad \Delta_R H^0 = 206\ \mathrm{kJ/mol} \tag{iv}$$

$$CH_4 + 2\ H_2O \rightleftharpoons 4\ H_2 + CO_2 \quad \Delta_R H^0 = 165\ \mathrm{kJ/mol} \tag{v}$$

$$CH_4 + CO_2 \rightleftharpoons 2\ H_2 + 2\ CO \quad \Delta_R H^0 = 247\ \mathrm{kJ/mol} \tag{vi}$$

Carbon formation is an unwanted side reaction. It can lead to a shutdown of the whole unit due to break-up of the catalyst particles, blocking of active sites and encapsulation of the pellets [17]. Carbon formation may occur in the rWGS reactor via equation (vii)-(ix) [17]. Carbon formation due to Boudouard reaction (viii) is thermodynamically favored at low temperature and elevated pressure whereas methane pyrolysis (vii) is favored at high temperature and low pressure. Hence, carbon formation can occur at very different operating conditions.

$$CH_4 \rightleftharpoons 2\ H_2 + C \quad \Delta_R H^0 = -75\ \mathrm{kJ/mol} \tag{vii}$$

$$2\ CO \rightleftharpoons CO_2 + C \quad \Delta_R H^0 = 172\ \mathrm{kJ/mol} \tag{Viii}$$

$$H_2 + CO \rightleftharpoons H_2O + C \quad \Delta_R H^0 = 131\ \mathrm{kJ/mol} \tag{ix}$$

It has to be pointed out that carbon formation cannot be ruled out only by assessing the equilibrium composition, as local concentrations and temperatures may still lead to high local carbon formation affinities [17]. Hence, to rule out carbon formation, further assessment would be required.

Although the rWGS feed composition changes with different rWGS

operating conditions, the general influence of pressure and temperature is shown in Fig. 2 and Fig. 3 for a fixed feed composition. The temperature dependent equilibrium composition is calculated in Aspen Plus® at 5 bar for a constant H_2/CO_2 ratio of 2 and for a molar feed stream of 1 mol/s. The resulting gas composition and the carbon formation rate are shown in Fig. 2. The CO content increases monotonously with the temperature because all CO forming reactions are endothermic. Methane formation is favored at low temperature (Equation (iv)-(vi)). The carbon formation rate decreases with increasing temperature until it becomes negligible. Consequently, the exothermic reactions (Equation (viii) and (ix)) are critical for carbon formation.

The CO yield Y_{CO} and CO selectivity S_{CO} are calculated as follows:

$$Y_{CO} = \frac{\dot{n}_{CO,out}}{\dot{n}_{CO2,in}} \quad (x)$$

$$S_{CO} = \frac{\dot{n}_{CO,out}}{\dot{n}_{CO2,in} - \dot{n}_{CO2,out}} \quad (xi)$$

The CO yield expresses the overall CO production from CO_2, whereas the selectivity is a measure for occurring side reactions. Fig. 3 shows the influence of pressure and temperature, for a constant H_2/CO_2 ratio of 2, on the CO yield and CO selectivity. Both increase with increasing temperature and decreasing pressure due to decreasing methane formation. Hence, higher temperatures are required for the same CO selectivity/yield when the pressure is increased. In the methane forming temperature range ($S_{CO} < 1$), the temperature dependency is very pronounced. Once the CO selectivity approaches unity, the temperature dependency on the CO yield is decreased. In this temperature range only the rWGS reaction occurs. In conclusion, minimizing pressure and maximizing temperature leads to higher CO yield/selectivity. As has been pointed out in the beginning of this section, the CO yield affects the tail gas recycle properties. Different tail gas properties lead to different split ratios to the burner, rWGS and FTS (compare Fig. 1), and hence, affect the whole process operation control.

Aim of this work

Different authors have applied different rWGS operating conditions in their PtL processes (see Chapter 1.2). However, no systematic study can be found in the literature on the selection of the rWGS operating conditions within a PtL concept. The aim of this work is to assess the impact of different operating conditions (pressure and temperature) in the rWGS reactor on the overall PtL process performance. Due to the different recycles in the PtL process (see Fig. 1), determining the optimum rWGS operating conditions is not straightforward. Changes in

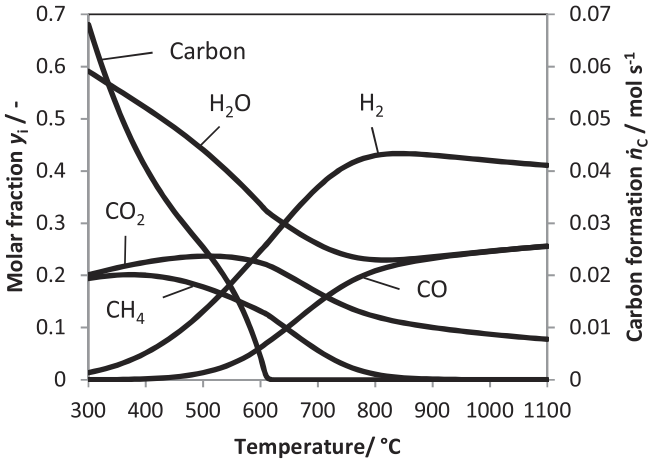

Fig. 2. Molar gas composition y_i and carbon formation rate $\dot{n}_C$ (graphite) for 300–1100 °C and 5 bar at thermodynamic equilibrium. Feed: 1 mol/s, $H_2/CO_2 = 2$.

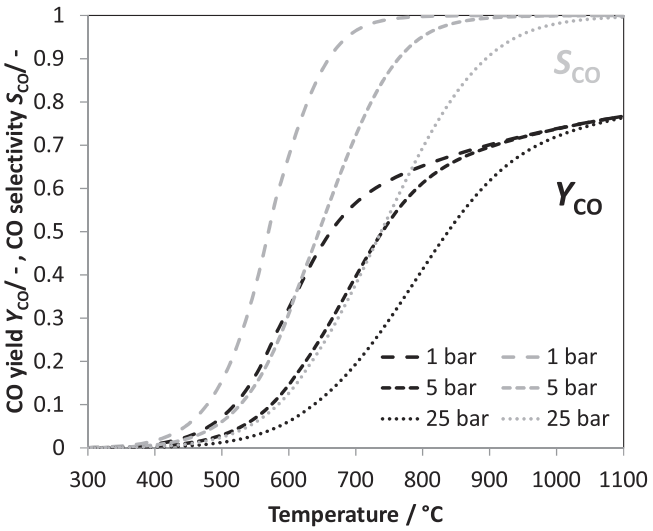

Fig. 3. CO yield (Y_{CO}) and CO selectivity (S_{CO}) at thermodynamic equilibrium for 300–1100 °C, 1–25 bar with an exemplary molar feed of $H_2/CO_2 = 2$. Increasing temperature and decreasing pressure leads to higher CO yields and CO selectivities.

rWGS pressure and temperature lead to changes in rWGS product distribution. This affects the recycle properties and thus, the split ratios towards FTS, burner and rWGS. For example, higher methane content in the rWGS product leads to higher recycling rates to the rWGS, which may affect the heat duty of the burner and consequently the fuel demand. The different influences lead to a set of favorable rWGS operating conditions. The objective of this work is to give an insight into the different correlations and to identify the best suited rWGS operating conditions to optimize the overall process performance. The process performance is investigated regarding:

- H-/C- efficiency: Amount of hydrogen from water/ carbon from CO_2 required for the fuel production.
- PtL-efficiency: Amount of electrical energy required to produce the desired liquid hydrocarbons.
- Pinch analysis: Assessment of heat integration possibilities.

In order to see how the optimum operating conditions are affected by the modelling assumptions, a sensitivity analysis is conducted.

Methodology

In the following chapter the modelling assumptions are defined. Chapter 2.1 describes the flowsheet and constraints in the general modelling approach. Chapter 2.2 deals with the assumptions of each process unit. In chapter 2.3 additional processing of the simulation results in Aspen Plus® using DLR's techno-economic process evaluation tool (TEPET) is explained. If not stated otherwise, temperature T and pressure p represent the temperature and pressure at the outlet of the rWGS reactor.

General modelling assumptions

The process is modelled in Aspen Plus®. The equation of state Peng-Robinson with Boston-Mathias modifications (PR-BM) is used, which is common for oil and gas production as well as hydrocarbon separation [18]. Chemical species involved in the model are H_2, CO, CO_2, H_2O, N_2, O_2 and alkanes (C_1-C_{30}, C_{32} representing C_{31}-C_{35}, C_{36} representing C_{36+}). Carbon formation in the rWGS reactor is not only affected by the thermodynamic equilibrium composition of the gas phase. The choice of catalyst as well as the concentration and the temperature profiles in the

actual reactor set-up affect the carbon formation, additionally [17]. It is beyond the scope of this work to investigate this in detail and to conclude whether carbon formation occurs. Thus, carbon is not included as a possible product.

The flowsheet is depicted in Fig. 4. The plant size is approximated to process the CO_2 emissions of an average German cement plant (~35.6 t_{CO2}/h calculated from [19]). In a first round of evaluation ($p_{rWGS} = 1$ bar, $T_{rWGS} = 725$ °C), the required hydrogen amount is calculated to 6 t_{H2}/h. It is worth mentioning, that this plant size requires a renewable base load power of 302 MW_{el} (see chapter 2.2 *Water electrolysis*) or 2.6 TWh p.a., which equals 0.56% of the installed wind power capacity (54 GW_{el} [20]) and 2 % of the wind power production in Germany in 2019 (131.8 TWh p.a. [20]). Although no water electrolyzers are in operation at this scale, chlor-alkali electrolysis is already available at large scale (typically 30–150 MW_{el} [21]), providing basic electrochemical know-how for large scale alkaline electrolysis [22]. Thyssenkrupp Industrial Solutions AG for example states, they could provide 10–20 MW_{el} modules (alkaline electrolysis) for a 100 MW_{el} plant and build 600 MW_{el} capacity each year [22]. In the following studies the hydrogen feed is kept constant, while the CO_2 feed varies with different rWGS operating conditions. The CO_2 feed is controlled to provide a constant molar ratio of $H_2/CO = 2$ in the feed of the FT reactor.

The aim is to produce syncrude for transportation fuels, especially targeting the kerosene and diesel range (C6-C21) [23]. To maximize the carbon efficiency, all gaseous components from the product separation are recycled. This recycle stream is split (S-1) as follows:

- The recycle to the FTS (Rec-FTS) is regulated to dilute the FT feed to have a constant inert gas content of 50 mol% (see chapter 2.2 *Fischer-Tropsch Synthesis*). Inert gas components are assumed to be all molecules except H_2 and CO.
- The recycle to the burner (Rec-Burn) is controlled to provide sufficient fuel and hence heat for the rWGS reactor.
- Remaining recycle gas is sent back to the rWGS (Rec-rWGS).

The flue gas from the burner is split (S-2) into three streams:

- The flue gas recycle to the burner is controlled to have a constant burner outlet temperature of 1200 °C [24,25].
- To account for impurities of the feed gases, a constant N_2 feed of 0.42 t/h is added to the hydrogen feed stream. This equals 0.36 vol-% of impurities based on the input of H_2, O_2 and CO_2. The overall impurity concentration is calculated with gas purities of 2.8 for H_2 and O_2 [26] and 2.0 for CO_2 [27]. The purge stream is controlled to have no accumulation of N_2 in the system.
- The remaining gas is sent back to the rWGS.

An overall pressure drop of 3 bar is assumed and implemented as a valve (V-1) in the recycle stream. The compressors are implemented as 3-staged compressors with an isentropic efficiency of 72 % and 100 % mechanical efficiency [28].

Unit description

CO_2 capture

Details on post combustion capture of CO_2 from cement plants can be found in [27]. Monoethanolamine (MEA) absorption is chosen, as it is a state-of-the-art technology (high maturity) for CO_2 capture [27]. MEA scrubbing is used in small plants producing up to 16.7 t CO_2/h for food, beverages and the chemical industry [27]. The downside of the MEA absorption process is a rather high thermal energy demand compared to other solvents under development [27]. As the exothermic FT reaction provides an excess of thermal energy, this energy can be used to provide the heat for CO_2 capture. The thermal energy demand for MEA absorption is 3.8 $MJ_{th}/kg\ CO_{2,\ captured}$ and the electricity required is 0.14 $MJ_{el}/kg\ CO_{2,\ captured}$ [29]. The desorption temperature is assumed to be constant at 120 °C for pinch analysis [29]. The CO_2 recovery ratio is 90 % [29] and the MEA outlet conditions of the stripped CO_2 after condensation are 1 bar and 25 °C [27].

Water electrolysis

Water electrolysis can be conducted in alkaline, proton exchange membrane (PEM) and solid oxide electrolysis cells, which are available at different levels of maturity [30]. PEM electrolysis is commercially available, but not in large scale applications [30]. However, PEM seems best suited for intermittent operation [30], which is crucial in most renewable electricity cases. Current PEM system efficiencies are in the range of 4.2–6.6 kWh_{el}/m^3_{H2} [30,31]. In this work an intermediate electrolysis efficiency of $\eta_{LHV} = 66.67$ % (≙ 4.47 kWh_{el}/m^3_{H2}) is assumed. The hydrogen feed is constant at 6.048 t/h (25 bar, 25 °C) for all scenarios (see chapter 2.1). Hence, 302 MW_{el} are required for the electrolysis. Current stack sizes range up to 2–3 MW_{el} [32]. Thema *et al.* reviewed the status-quo on existing Power-to-Gas plants in terms of hydrogen and methane production from electricity. In early 2019, the globally active Power-to-Gas projects comprise an electrical power input of 38.6 MW_{el} (electrical input for electrolysis) [33]. Hence, 8 times the globally produced hydrogen from electricity would be required for this plant. However, work is ongoing to bring the technology to the > 100 MW scale [33].

CO_2 activation

The rWGS reactor is modelled as a Gibbs reactor (Gibbs minimization) and thereby assuming thermodynamic equilibrium at the

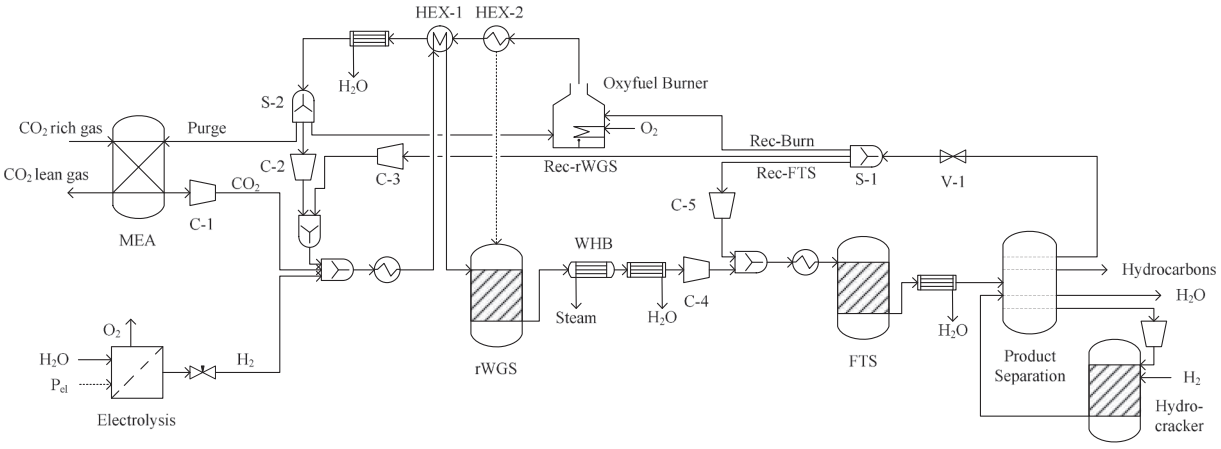

Fig. 4. Flowsheet of the PtL model in Aspen Plus® including monoethanolamine absorption (MEA), waste heat boiler (WHB), compressors (C), splits (S), heat exchangers (HEX) and valves (V).

respective outlet temperature and pressure of the reactor [13]. The operating conditions are varied from 550 to 950 °C and 1–25 bar (see chapter 3.1). It is assumed that the product stream cannot be used for preheating the feed stream, as its properties are prone to metal dusting (metal dusting occurs at high CO concentration and 450–800 °C [34]). Alternatively, the product gas is used in a waste heat boiler (WHB) to produce high pressure steam. In a WHB the heat transfer resistance is mainly at the product gas side and the wall temperature is close to the steam temperature [34]. With these low wall temperatures the risk of metal dusting is rather low [34].

Oxyfuel burner

To decrease the amount of inert gas in the process, the by-product oxygen from the electrolysis is used in an oxyfuel burner (instead of combustion with air). The burner, operated at 1 bar, provides the heat for the endothermic rWGS reactor. Complete combustion (stoichiometric reactor) is assumed with $\lambda = 1$. The cold flue gas is recycled back to the burner to have a constant, adiabatic, outlet temperature of $T_{\mathrm{Burn}} = 1200$ °C [24,25]. A flameless oxyfuel burner, providing 40 MW_{th}, is in operation in Sweden [25]. This configuration is well in line with the thermal energy demand in this work (compare Fig. 8). The outlet temperature of HEX-2 ($T_{\mathrm{HEX\text{-}2}}$ in °C) is calculated from the rWGS reactor outlet temperature (T_{rWGS} in °C) according to:

$$T_{\mathrm{HEX-2}} = T_{\mathrm{rWGS}} + \Delta T \tag{xii}$$

$$\Delta T = 340\ ^{\circ}\mathrm{C} - \frac{T_{\mathrm{rWGS}}}{5} \tag{xiii}$$

Equation (xiii) is approximated from tubular steam-methane reforming:

- Reformer exit temperature: 700–950 °C [17] (here: T_{rWGS}) and the according
- Flue gas exit temperature: 900–1100 °C [17] (here: $T_{\mathrm{HEX\text{-}2}}$)

The flue gas leaving the combustion chamber (HEX-2) is then further used to heat the rWGS feed in a countercurrent heat exchanger (HEX-1), with a Hot_{out} - $Cold_{in}$ temperature difference of 50 K (U-value = 50 W/m^2K [35]). In some cases this specification leads to a temperature cross in the heat exchanger. The specification is then set to 50 K for the temperature difference of Hot_{in}- $Cold_{out}$ instead. As the CO concentrations in the flue gas and rWGS feed are low, minor risk for metal dusting in HEX-1 is expected.

Fischer-Tropsch synthesis

A tubular fixed bed reactor with cobalt catalyst, only alkanes as product [16], is assumed. This kind of reactor is, for example, used in the GtL plant in Bintulu, Malaysia [36]. This plant uses Shell Middle Distillate Synthesis (SMDS) technology and is about 5 times of the size of the reactor in this work [36]. However, the fixed bed reactor is comparably easy to scale [37]. The rWGS product stream is cooled (40 °C) to separate most of the water as steam may cause deactivation on cobalt catalysts [38]. The Fischer-Tropsch reactor is modelled as a stoichiometric reactor at 25 bar and 220 °C [39]. The H_2/CO ratio is fixed to 2 [36]. Under these conditions the chain growth probability α is calculated according to equation (xiv) to 0.839 [40]. The methane selectivity is $S_{CH4} = 0.161$ [40].

$$\alpha = \frac{1}{1 + 0.0567\left(\frac{c_{H2}}{c_{CO}}\right)^{1.76} \exp\left(3620\ \mathrm{K}\left(\frac{1}{493.15\ \mathrm{K}}\right) - \left(\frac{1}{T}\right)\right)} \tag{xiv}$$

The CO conversion is assumed to be 40 % [41] and the inert gas share is fixed, conservatively, to 50 % [42] to prevent catalyst deactivation, decreasing selectivity and thermal runaway due to strong non-isothermal behavior [39].

Hydrocracker

To increase the yield towards liquid fuels, the heavy hydrocarbons (liquid fraction at 150 °C, 25 bar) are fed to a hydrocracker. The required hydrogen amount is calculated to satisfy the H/C ratio of the alkanes at the outlet of the hydrocracker. The reactor is modelled as a yield reactor at 35 bar and 370 °C [43]. A polynomial yield curve is approximated with a combination of yields for C_1-C_{10} taken from [44] and C_{10}-C_{30} taken from [43].

Product separation

In a first flash (150 °C, 25 bar) the heavy hydrocarbons are separated from the FT product stream and sent to the hydrocracker. The product from the hydrocracker is then added to the product separation, which consists of 8 flashes at 4 fixed temperatures (110 °C, 70 °C, 40 °C, −15 °C) and 2 pressures (25 bar, 1 bar) [13]. The main products of the separation are water, recycling gases (gaseous compounds at: 110 °C, 70 °C, 40 °C, −15 °C at 1 bar and −15 °C at 25 bar) and the desired synthetic hydrocarbons.

Validity of the process model

To our knowledge, there is no experimental data available in the literature for the exact same configuration as described in this work. Hence, the validation of the proposed overall PtL process concept is still pending. For the assessment of the entire PtL process, valid models for the FT reactor and for the rWGS reactor including the burner unit are essential. The FT model used in this study was proposed and fitted for a broad range of FT operating conditions by [40]: $T_{\mathrm{FTS}} = 470$–530 K, $p_{\mathrm{FTS}} = 12$–36 bar, syngas ratio in the bulk = 0.1–3.0, H_2/CO = 1–3. The FT operating conditions in this work are within the given boundaries for the fitted model. Further information on the validity of the FT model results can be found in [40]. The sensitivity of the rWGS reactor model on changing rWGS operating conditions is of high importance in this work. Thermodynamic equilibrium is assumed, as has been applied in previous studies [13,38]. In [45], kinetic experiments are conducted using a monolithic, noble metal catalyst at 1.5 bar for different H_2, CO_2 and CH_4 feeds at different temperatures (600–900 °C) and at a high residence time. The equilibrium composition calculated in Aspen Plus® matches the experimental results, if carbon formation is suppressed in the simulation [45]. The calculation of the burner temperature is based on empirical data for methane steam reforming. Although this seems reasonable, as both reactor types show a lot of similarities, a more detailed model or experimental validation would be beneficial to proof this assumption.

TEPET

The Aspen Plus® simulations are supported by DLR's 'Techno-Economic Process Evaluation Tool' (TEPET) [46]. Apart from the possibility to evaluate process economics, details see [46], this tool improves the handling of technical evaluations based on Aspen Plus® simulations. With TEPET's 'simulation control' it is possible to vary parameters in Aspen Plus®, for example operating conditions of a unit, while saving the results of each simulation run. This increases efficiency in data collection. As there are different recycles within this Aspen Plus® simulation, TEPET's 'open loops' is used to speed up convergence, even under severe changes in operating conditions. Automatic pinch analysis is carried out in TEPET's 'heat integration', using T-H curves derived from Aspen Plus®. Automatic heat integration allows estimating the amount of required cooling media or possible steam production from excess thermal energy without extensive heat exchanger networks.

Results and discussion

Chapter 3.1 to 3.5 deal with the base case as described in chapter 2. Chapter 3.1 addresses the limitations of the operating window of the

rWGS in the PtL process. In chapter 3.2 and 3.4 the influence of the rWGS operating conditions on the product output and Power-to-Liquid efficiency is analyzed and correlations are outlined in detail. Chapter 3.3 covers the carbon and hydrogen efficiency and chapter 3.5 gives insight into different heat integration options for one specific case. In chapter 3.6 sensitivity analysis is conducted to analyze the effect of the assumptions on the optimum operating conditions.

Operating window

The investigated rWGS pressure range is 1–25 bar. The lower pressure boundary of 1 bar is selected because lower pressure increases the CO-yield (see chapter 1.3). To reduce the required energy for compression, the upper pressure boundary is equal to the FTS operating pressure (25 bar). The investigated rWGS temperature range is between 550 and 950 °C. The maximum temperature is selected due to material considerations. The lower temperature boundary is restricted by the assumption of 50 mol% inert gas content in the FTS feed. The recycle to the FTS (Rec-FTS) varies strongly for different rWGS operating conditions (Fig. 5). With decreasing rWGS temperature and increasing rWGS pressure the methane content in the rWGS product stream increases. Hence, less gas is recycled back to the FTS (Rec-FTS) to provide the constant inert gas content in the feed of the FTS. At a certain temperature the recycle ratio to the FTS approaches zero. Below this temperature, the inert gas content exceeds the fixed molar share of 50 %. Thus, for 1 bar, 5 bar, 10 bar and 25 bar, the respective rWGS minimum temperature is 581 °C, 670 °C, 714 °C and 780 °C.

Product output

The product output $\dot{m}_{\text{Hydrocarbons}}$ is the lumped hydrocarbon output of all liquid fractions (see stream "Hydrocarbons" in Fig. 4). An example for the hydrocarbon product distribution is shown in Fig. 6.

The dependency of the product output on the rWGS operating conditions is shown in Fig. 7. Starting at low temperature, the product output increases until it reaches a maximum. The maximum output (10.21 t/h) is obtained at 1 bar and 725 °C. Increasing the temperature further, shows first a slight decrease in product output, until the product output decreases again significantly. Streams leaving the system boundaries are water, purge gas and hydrocarbon product. Higher hydrocarbon product yields are achieved when purge gas and water production decrease. Conclusively, the product output correlates inversely with the water production and purged gas. Steam from combustion,

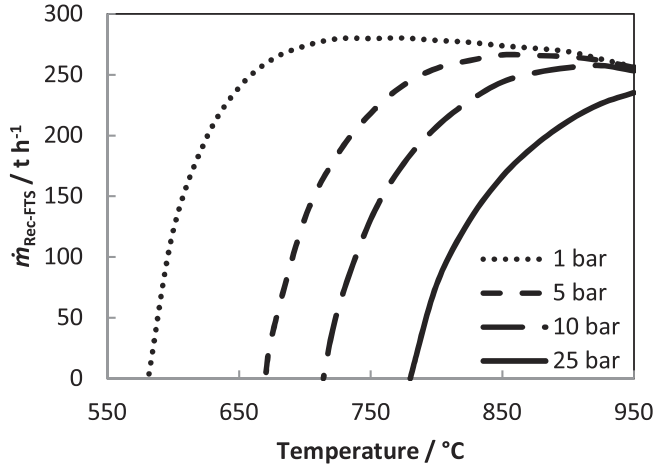

Fig. 5. Mass flow rate of the recycle stream from the product separation to the FTS $\dot{m}_{\text{REC-FTS}}$ for different rWGS pressures and temperatures. Pressure dependent lower rWGS boundary temperature, where FTS recycle stream approaches zero.

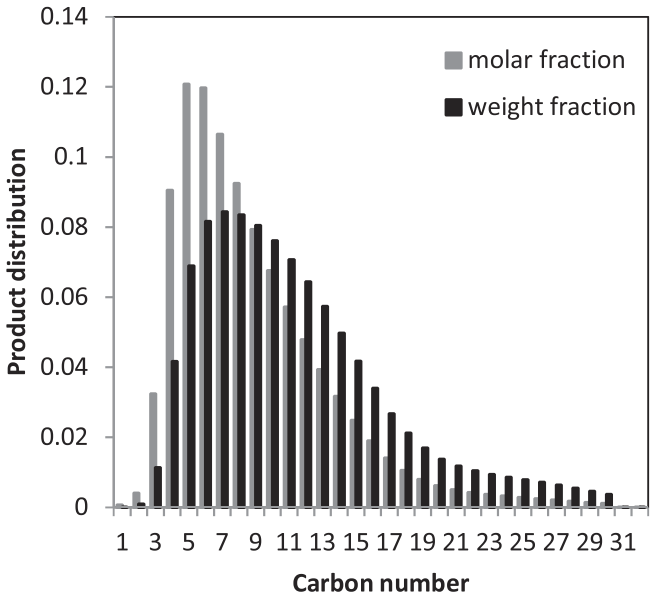

Fig. 6. Hydrocarbon product distribution (stream "Hyrocarbons" in Fig. 4) at $p_{\text{rWGS}} = 5$ bar and $T_{\text{rWGS}} = 825$ °C.

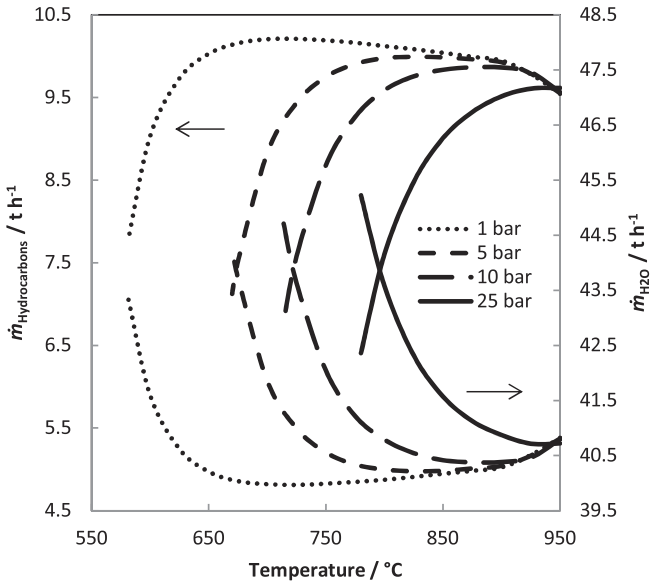

Fig. 7. Lumped hydrocarbon product output $\dot{m}_{\text{Hydrocarbons}}$ and water output $\dot{m}_{\text{H2O}}$ for different rWGS pressures and temperatures. The hydrocarbon output correlates with the water exiting the system boundaries.

rWGS reaction and FTS is condensed and separated from the process (compare Fig. 4). Hence, hydrogen forming steam is no longer available for the hydrocarbon production. Fig. 7 shows the amount of water $\dot{m}_{\text{H2O}}$ exiting the system boundaries. It is evident, that the product output correlates inversely with the amount of water produced. In contrast, CO_2 (e.g. from CO combustion) is recycled via MEA absorption. As 90 % of the purged CO_2 is recovered in the MEA unit, the amount of purge gas has only minor influence on the product output.

The overall water production depends on:

- the heat duty $\dot{Q}_{\text{rWGS}}$ required for preheating and for the endothermic reaction in the rWGS reactor,
- the composition (atomic hydrogen content β) of the fuel gas recycled to the burner (Rec-Burn) and

- the recuperation efficiency of HEX-1.

The heat demand of the rWGS reactor is shown in Fig. 8. It is the summation of heat required for preheating from 450 °C to rWGS reaction temperature plus the heat required for the endothermic reaction. For a given pressure there is an optimum temperature with minimum heat demand. Above this optimum temperature the heat demand increases slightly due to the increase in $\Delta T = T_{\mathrm{rWGS,\ out}} - T_{\mathrm{rWGS,\ in}}$. Decreasing the temperature leads to higher methane concentrations in the recycle and therefore higher recycle rates to the rWGS (Rec-rWGS). Hence, for temperatures lower than the optimum temperature, the heat demand increases due to a higher throughput that has to be heated up. The heat demand varies in the range of 28–49 MW_{th} and the minimum heat requirement is found at 625 °C and 1 bar.

Intuitively, higher heat demand leads to higher water production. However, for low and high rWGS temperatures the correlation between rWGS heat duty and overall water production shows deviations.

The combustion reaction of a hydrocarbon mixture is shown in equation (xv). From the stoichiometry of this reaction, it is evident, that a change in the recycle gas composition, thus burner fuel composition, influences the amount of water produced in the burner. For low rWGS temperatures the methane content in the recycle increases significantly, which leads to significant changes in burner fuel composition. This increase in methane content leads to an increase in β and consequently water production. Fig. 8 shows the atomic hydrogen content β for different rWGS pressures and temperatures. The higher methane content in the burner fuel leads to a prominent increase in water production at low rWGS temperatures, e.g. at 1 bar below 650 °C. Minimum β is found at 1 bar and 800 °C. As the minimum rWGS heat duty is obtained at 625 °C and the minimum β at 800 °C, the minimum overall water production is achieved between these temperatures at 725 °C.

$$C_\alpha H_\beta O_\gamma + \left(\alpha + \frac{\beta}{4} - \frac{\gamma}{2}\right) O_2 \rightarrow \alpha\, CO_2 + \frac{\beta}{2}\, H_2O \qquad \text{(xv)}$$

The heat exchanger preheating the rWGS feed with the flue gas (HEX-1) is specified to reach a temperature difference of 50 K for the Hot_{out}- $Cold_{in}$ streams (see chapter 2.2). For high temperatures (≥ 900 °C at 1 bar, 925 °C at 5 bar, 925 °C at 10 bar, 950 °C at 25 bar) this specification leads to a temperature cross in the heat exchanger. Under these rWGS operating conditions the heat exchanger is calculated to satisfy a temperature difference of 50 K for the Hot_{in}- $Cold_{out}$ streams. Consequently, the energy in the flue gas cannot be fully utilized, resulting in higher outlet temperatures of the hot stream and thus a higher thermal waste stream. Additional fuel is burned, as the flue gas is not fully recuperated, which leads to an increase in water production.

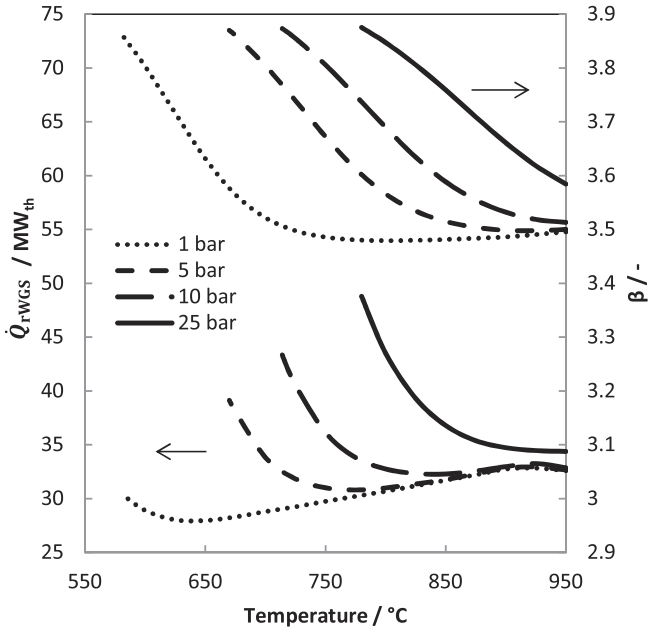

Fig. 8. Left: Heat demand of the rWGS unit $\dot{Q}_{rWGS}$ for different rWGS temperatures and pressures. Low temperatures lead to higher methane content in the recycle and thus higher recycle rates to the rWGS (Rec-rWGS). This increases the rWGS feed that requires heating up. Right: β (atomic hydrogen content in the recycle) as a function of rWGS temperature and pressure. Low temperatures lead to high methane content and thus higher β.

Carbon and hydrogen efficiency

Carbon enters the system boundaries as CO_2, flue gas from the cement plant ($\dot{n}_{C,\ \mathrm{Cement\ Plant}}$), and leaves the system boundaries as hydrocarbon product ($\dot{n}_{C,\ \mathrm{Hydrocarbons}}$), purge gas or dissolved in water. The amount of carbonaceous molecules dissolved in water is comparably low to the amount of carbon in the hydrocarbon product and purge gas. For calculating the carbon efficiency, the carbon incorporated in the hydrocarbon product is set in relation to the amount of carbon from the cement plant (equation (xvi)):

$$\eta_C = \frac{\dot{n}_{C,\ \mathrm{Hydrocarbons}}}{\dot{n}_{C,\ \mathrm{Plant}}} \qquad \text{(xvi)}$$

As both, the flue gas from the cement plant and the purge gas, are processed by the MEA unit, the performance of the MEA absorption has a large influence on the carbon efficiency. The MEA recovery rate is independent of the rWGS operating conditions. 10 % of the CO_2 from the cement plant and purge gas cannot be recovered (as a recovery rate of 90 % is assumed in chapter 2.2). The carbon efficiency obtained equals η_C = 88 % (Fig. 9) and is not affected by changes in rWGS operating conditions. The carbon dioxide amount required from the cement plant is shown in Fig. 9. The CO_2 stream correlates directly with the product output (compare Fig. 7). Higher product output leads to an increase in$\dot{m}_{CO2,\ \mathrm{Cement\ Plant}}$, as the H_2/CO ratio in the feed of the FTS is assumed to be constant. Overall, this leads to a constant C-efficiency.

The hydrogen efficiency is calculated according to equation (xix) from the atomic hydrogen amount in the hydrocarbon product

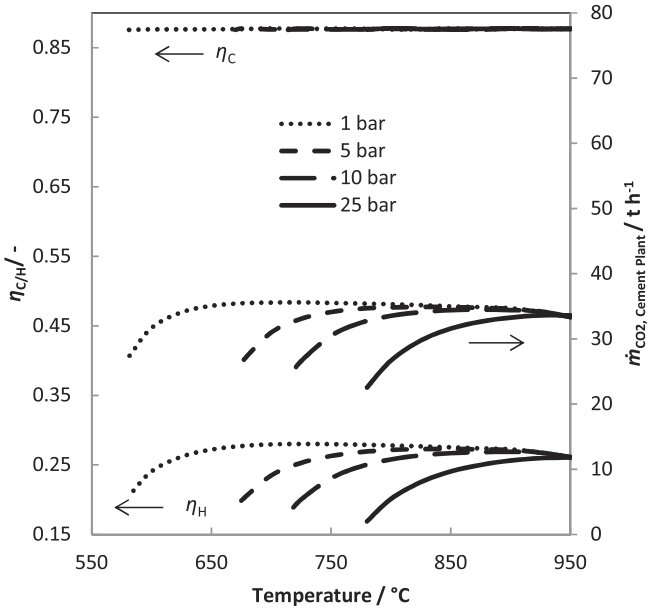

Fig. 9. Left: Hydrogen and carbon efficiency for different rWGS pressures and temperatures. η_H correlates inversely with the water production (compare Fig. 7). The carbon efficiency is not affected by the rWGS operating conditions. Right: CO_2 demand from the cement plant. The carbon dioxide demand correlates with the product output (compare Fig. 7).

($\dot{n}_{H,\ Hydrocarbons}$) and the atomic hydrogen amount in the electrolysis feed ($\dot{n}_{H,\ Electrolysis}$).

$$\eta_H = \frac{\dot{n}_{H,\ Hydrocarbons}}{\dot{n}_{H,\ Electrolysis}} \quad \text{(xvii)}$$

Hydrogen enters the system boundaries as water (feed to electrolysis) and leaves the boundaries as water (condensed steam) or hydrocarbon. As the hydrogen input is constant, the hydrogen efficiency (Fig. 9) correlates inversely with the water production (compare Fig. 7).

Power-to-Liquid efficiency

Electrolysis, MEA and compressors are the major contributors to the overall power consumption of the process. Hence, the Power-to-Liquid efficiency is calculated as follows:

$$\eta_{PtL} = \frac{\dot{m}_{Hydrocarbons}\ LHV_{Hydrocarbons}}{P_{Electrolysis} + P_{MEA} + P_{Compression}} \quad \text{(xviii)}$$

The efficiency is calculated from the lumped mass flow of the overall hydrocarbon output ($\dot{m}_{Hydrocarbons}$), the lower heating value of the overall hydrocarbon output ($LHV_{Hydrocarbons}$) and the electrical energy input for electrolysis ($P_{Electrolysis}$), MEA (P_{MEA}) and compression ($P_{Compression}$).

As the hydrogen input is constant in this study, the power demand for the electrolysis is constant (302 MW_{el}). The electricity demand for MEA absorption varies with the amount of $CO_{2,\ captured}$, between 1.0 and 1.55 MW_{el} (see Fig. 10). Hence, CO_2 capture has only a minor share of the overall electrical energy input. Compression work varies between 4 and 51 MW_{el} due to different gas flow rates and pressure levels. If the rWGS is operated at low pressure this increases the compression work in compressor C-4 (see Fig. 4). Operating the rWGS at 25 bar decreases the compression work, as the FTS and rWGS are operated at the same pressure level and thus no additional compression work is required. Decreasing the rWGS temperature leads to higher methane content and thus, higher recycling rates to the rWGS (Rec-rWGS). Therefore lower temperatures require more electrical energy for compression.

Fig. 11 shows the resulting PtL-efficiency at different rWGS temperatures and pressures. The PtL-efficiency varies between 25.4 % and 38.7 %. For a given pressure, there is a plateau, where the PtL-efficiency is only affected marginally by the rWGS temperature. The according

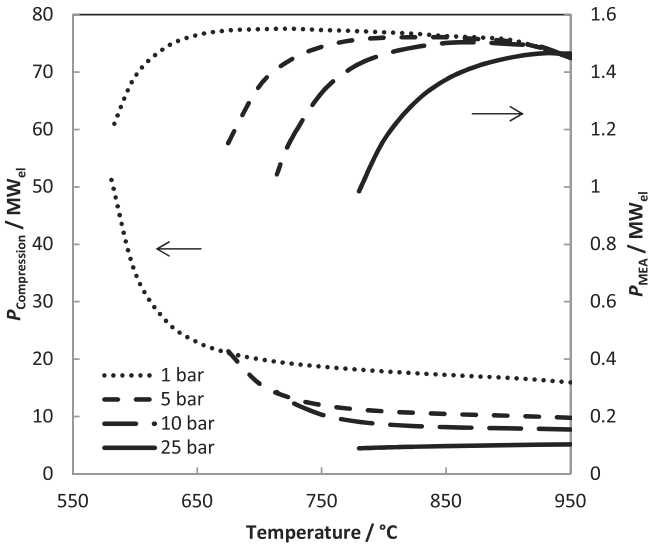

Fig. 10. Electricity demand required for compression $P_{compression}$ and monoethanolamine absorption P_{MEA} for different rWGS temperatures and pressures. P_{MEA} is comparably low to $P_{compression}$. $P_{compression}$ increases with decreasing pressure and temperature.

rWGS temperatures and pressures for a relative decrease of 1 % and 3 % PtL-efficiency are shown in Fig. 11 on the right side. The maximum PtL-efficiency is found at 5 bar and 825 °C:

$$\eta_{PtL}(5\ bar,\ 825\ ^{\circ}C) = \frac{2.77\ \frac{kg}{s} \cdot 43.85\ \frac{MJ}{kg}}{302\ MW + 1.5\ MW + 10.6\ MW} = 0.387$$

Analogous to the product output (compare chapter 3.2), the PtL-efficiency has an optimum temperature for a given pressure. However, the maximum product output is found at 1 bar and 725 °C (chapter 3.2) and the maximum PtL-efficiency is obtained at 5 bar and 825 °C. The increase in optimum pressure in terms of energetic efficiency corresponds to the higher compression work at lower pressures (compare Fig. 10). Hence, 5 bar is energetically favored over 1 bar. The higher optimum temperature from the energetic perspective is due to the increase in methane formation at higher pressure which requires higher temperatures for the same CO-yield.

Heat integration

Automated pinch analysis is conducted for all cases (see chapter 2.3). The pinch temperature difference is fixed to 10 K. Burner and rWGS reactor are not included in the pinch diagram as the thermal coupling is already performed in the Aspen Plus® simulation. One exemplary pinch analysis is shown in Fig. 12 for 5 bar and 825 °C (as this case has the maximum PtL-efficiency, see chapter 3.4). The diagram includes two curves: the summation of all hot streams ('hot stream'), which are available for heating or require active cooling, and the summation of all cold streams ('cold stream'), which require heating.

In this case, the heat from the exothermic FT reaction (39.5 MW_{th} at ~ 211 °C) is sufficient to provide enough heat for CO_2 absorption (31.6 MW_{th} at 120 °C). Below 100 °C active cooling is required (40 MW). As described in chapter 2.2, syngas leaving the rWGS reactor is cooled using a waste heat boiler. Most of this high temperature heat cannot be integrated in the process (20 MW_{th} at 370 °C-825 °C). One option to use this valuable high temperature heat is to produce electricity via a steam based Clausius-Rankine cycle 'SCR' (43 % efficiency, steam cycle modelled in Aspen Plus®). This scenario provides 15.8 MW_{el} and requires 1030 kg/s of cooling water ('CW'). The electricity regained from the Clausius-Rankine cycle can be used to decrease the power demand and hence increase the Power-to-Liquid efficiency:

$$\eta_{PtL,\ SCR} = \frac{\dot{m}_{Hydrocarbons}\ LHV_{Hydrocarbons}}{P_{Electrolysis} + P_{MEA} + P_{Compression} - P_{SCR}} \quad \text{(xix)}$$

This increases the PtL-efficiency from 38.7 % to 40.75 % (at 5 bar and 825 °C). Fig. 13 shows the efficiencies calculated with SCR for different rWGS pressures and temperatures. Compared to the PtL base case, the Clausius-Rankine cycle increases the PtL-efficiency by (ηPtL, SCR - η_{PtL} =) 1.6– 3.7 %. However, adding a Clausius-Rankine cycle to the PtL plant has yet to be proven to be economically beneficial. Another option to use the high temperature heat is high pressure steam (35.5 bar) production. The resulting 'cold stream' (at 5 bar and 825 °C) is shown in the pinch diagram in Fig. 12. This configuration produces 14.35 kg/s of steam and requires 906 kg/s cooling water.

Sensitivity studies

The findings in the previous subchapters result from the assumptions in chapter 2 (base case configuration). The assumptions described in chapter 2 are based on reasonable engineering guesses. Still, they may vary under different circumstances in a reasonable range. This might affect the overall optimum rWGS operating conditions. To investigate the influence of the most relevant assumptions on the optimum rWGS operating conditions, respective η_{PtL}, η_H, η_C, local sensitivity studies are conducted as depicted in Table 1.

Variables 1) and 2) do not influence the process streams and, thus, η_H

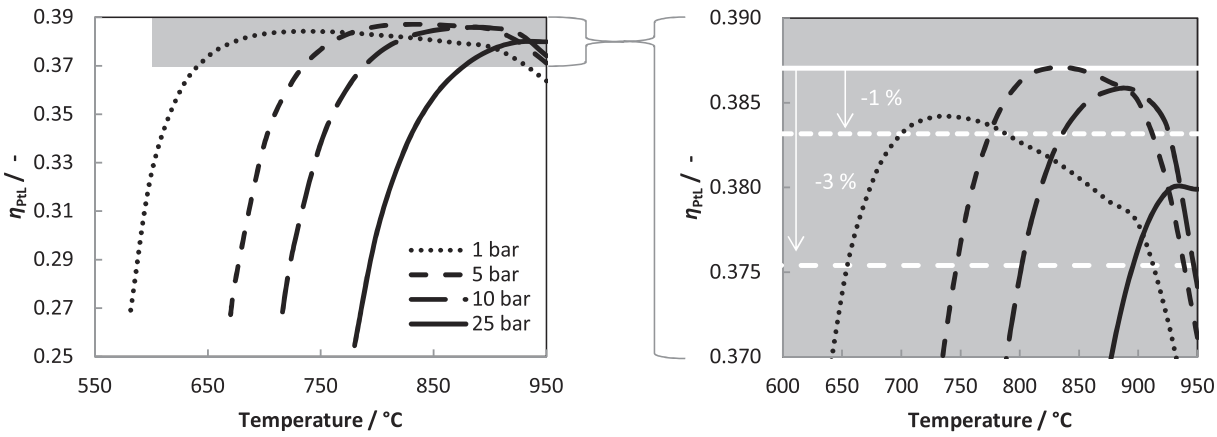

Fig. 11. Power-to-Liquid efficiency for different rWGS pressures and temperatures. Below and above a certain temperature, the PtL-efficiency decreases significantly.

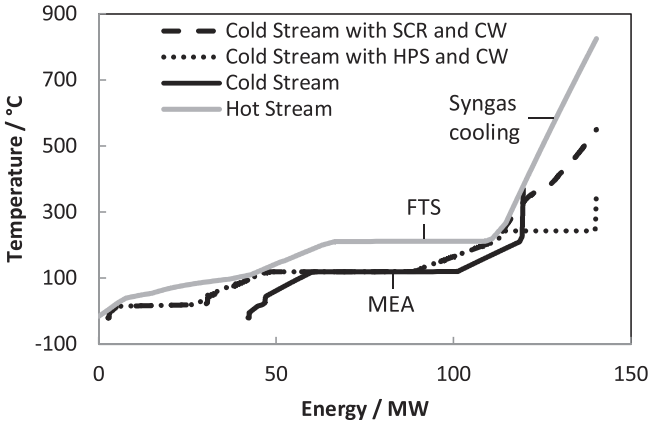

Fig. 12. Pinch analysis conducted at 825 °C rWGS temperature and 5 bar rWGS pressure. Major contributors to the "hot stream" are Syngas cooling and Fischer-Tropsch synthesis (FTS). The "cold stream" shows heat integration possibilities at high temperature. Thus, in one case a clausius-rankine cycle (SCR) and in a second case high pressure steam production (HPS) is integrated. Both cases include the cooling water demand (CW).

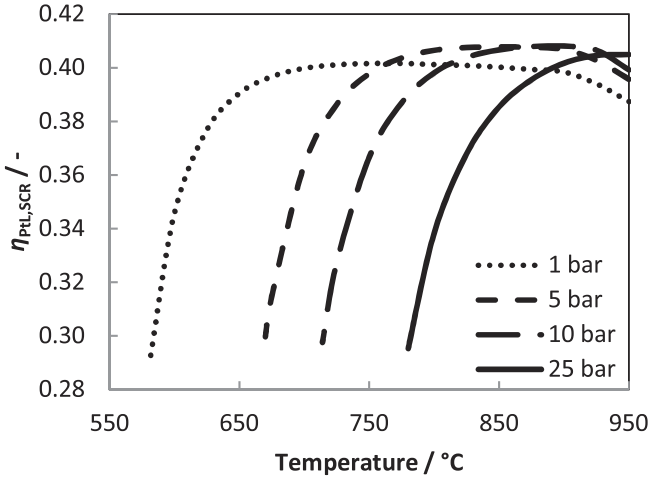

Fig. 13. Power-to-Liquid efficiency including clausius-rankine cycle at different rWGS pressures and temperatures. The PtL-efficiency can be increased by 1.6–3.7 % in comparison to Fig. 11.

Table 1
Variables for the sensitivity study related to the feed supply (1), 3)), rWGS + burner setup (4)-5)) and FTS performance (6)-9)). The α values are calculated with equation (xiv).

Variable	Min	Base	Max
1) $\eta_{Electrolysis,LHV}$ / -	0.6	0.667	0.7
2) $\eta_{Compression}$ / -	0.6	0.72	0.9
3) N_2 / t h^{-1}	0.042	0.42	–
4) ΔT_{HEX-1} / K	10	50	100
5) T_{Burn} / °C	1150	1200	1400
6) x / -	0.4	0.5	–
7) H_2/CO / (α/-)	1.8 (0.862)	2 (0.839)	2.2 (0.815)
8) T_{FTS} / (α /-)	210 (0.905)	220 (0.839)	225 (0.795)
9) X_{CO} / -	–	0.4	0.6

and η_C. However, they affect η_{PtL} directly as the electrolysis has a major share of the total energy input and the compression work has a significant effect on the optimum operating conditions (see chapter 3.4). The efficiency of the electrolyzer is varied between 57 and 47 kWh_{el}/kgH_2 [31], which equals $\eta_{Electrolysis,LHV}$ = 60–70 %. Varying the compressor efficiency can also be interpreted as a change in the overall pressure drop for a constant compressor efficiency. Variable 3) accounts for impurities in the feed streams (H_2, CO_2 and O_2) and may affect the process streams due to changes in partial pressures and hence rWGS product composition. As the base case has already been chosen conservatively, the N_2 feed is calculated for purities of 4.0 for H_2 and O_2 [26] and 3.0 for CO_2 [27]. Variables 4) – 5) influence the overall allothermal rWGS (rWGS + burner) configuration. They are prone to have a significant influence on the product output as they influence the heat duty of the burner. For example, decreasing the temperature difference in the heat exchanger HEX-1 will lead to an increase in heat transfer in HEX-1. Hence, the temperature of the rWGS feed stream increases and less thermal energy has to be provided by HEX-2. Thus, less fuel is consumed, which leads to lower water production and higher product output (compare chapter 3.2). Variables 6) – 9) represent changes in Fischer-Tropsch performance. The FTS temperature and the H_2/CO ratio in the FTS feed influence the chain growth probability α. Lower α leads to higher methane concentrations and hence more water production, which results in less product output (compare chapter 3.2). In addition, different H_2/CO ratios influence the CO_2 feed and hence all process stream properties. All FTS parameter have the ability to change the product distribution, which affects the recycle properties and consequently the product output.

Chapter 3.1 points out the lower rWGS temperature boundary, which is reached when the recycle to the FTS (REC-FTS) approaches zero. In contrast to that, an upper rWGS temperature boundary is found for specific cases marked with "u.b." in Fig. 15 and Fig. 16. In these cases the

recycle to the rWGS (Rec-rWGS) approaches zero and the inert gas content exceeds the fixed content of 50 mol%. Although it might be possible to operate the FTS with a higher reactants content than 50 %, these cases are marked as the upper temperature boundary, as they cannot be compared directly to the other cases.

Fig. 14 compares the deviation of the maximum PtL-efficiencies, calculated for the different variable values in Table 1, to the base case. The maximum PtL-efficiency is observed at $T_{rWGS} = 825$ °C and $p_{rWGS} = 5$ bar for almost all variations, except for $H_2/CO = 2.2$. In this case the optimum is observed at slightly higher rWGS temperature (850 °C). The overall maximum PtL-efficiency is found at low FTS temperature $T_{FTS} = 210$ °C ($\eta_{PtL} = 40.9\%$). In general, the PtL-efficiency increases with increasing $\eta_{Electrolysis}$, T_{Burn}, $\eta_{Compression}$, X_{CO}, x_{inert} and decreasing T_{FTS}, H_2/CO, ΔT_{HEX-1}. The efficiency of the electrolyzer $\eta_{Electrolysis}$, the FTS temperature T_{FTS} and the H_2/CO ratio in the feed of the FTS reactor have the highest influence on the PtL-efficiency. Decreasing T_{FTS} and the H_2/CO ratio leads to an increase in chain growth probability. For longer chains, less water is produced per hydrogen atom integrated in the hydrocarbon product. This decrease in water production leads to the increase in PtL-efficiency. It should be mentioned that the model for α (equation (xiv)) does not account for differences in inert gas content. This seems reasonable, as the experimental results from [47] show only minor influence of the inert gas content on α. Impurities and X_{CO} are found to have only minor influence on the PtL-efficiency. However, it is worth noting that, in this work, α is independent of the CO conversion. In contrast, [48] state that the methane selectivity decreases with increasing CO conversion. They also state that the influence of the FT reactor temperature is larger than the influence of the CO conversion [48]. Hence, if the model was to include the X_{CO} and α correlation, we would expect an increase in PtL-efficiency, although the difference should not be as pronounced as for a lower FT temperature.

Fig. 15 shows the according Power-to-Liquid efficiencies for the different variables at varying rWGS pressures and rWGS temperatures. Evidently, different assumptions for the variables in Table 1 lead to different Power-to-Liquid efficiencies for a given rWGS pressure and rWGS temperature combination. The ranges of the PtL-efficiency, for a given set of assumptions, are highlighted in 3 different grey tones. Dark grey shows the range from maximum PtL-efficiency to 0.1 % of the respective maximum efficiency. Light grey indicates the range of 1–3 %

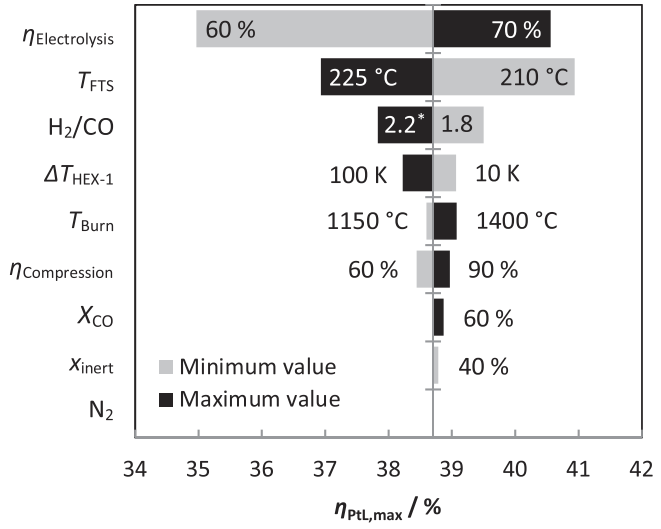

Fig. 14. Influence of the different variables from Table 1 on the maximum PtL-efficiency in terms of deviation from the base case (base case: $\eta_{PtL,max} = 38.7\%$). Black bars indicate an increase in variable value and grey bars a decrease in variable value. The optimum rWGS operating conditions (maximum PtL-efficiency) are found at $p_{rWGS} = 5$ bar and $T_{rWGS} = 825$ °C, except for the case with *$H_2/CO = 2.2$, where the optimum temperature is at $T_{rWGS} = 850$ °C.

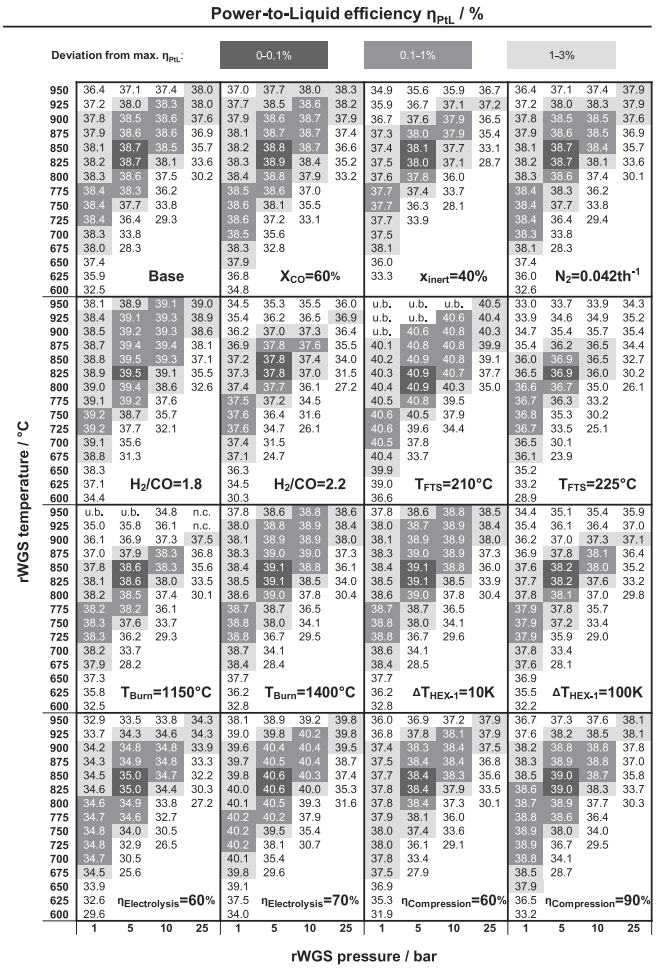

Fig. 15. Power-to-Liquid efficiency for different assumptions, rWGS pressures and rWGS temperatures. N.c. – not converged: No value available for the given constellation. U.b. – upper boundary: Rec-rWGS approaches zero and the inert gas content exceeds the fixed 50 mol%.

and medium grey of 0.1–1 %. The dark grey rWGS temperature and pressure constellations are not affected significantly by the variation of the variables. Remarkably, 5 bar and 825 °C (the optimum operating conditions for the base case) are included in the optimum operating conditions throughout the whole variation. This indicates that the optimum found for the base case is surprisingly robust. For increasing H_2/CO, T_{FTS} and decreasing T_{Burn}, ΔT_{HEX-1} the optimum window is comparably narrow whereas the inverse flattens the influence of the rWGS operating conditions leading to a broad range of rWGS operating conditions within the light grey range. The correlation of HEX-1 and HEX-2 becomes evident when comparing T_{Burn} and ΔT_{HEX-1}. Similar efficiencies, for a fixed rWGS pressure and temperature, are found for $T_{Burn} = 1400$ °C and $\Delta T_{HEX-1} = 10$ K. Increasing the burner temperature from 1200 °C to 1400 °C leads to an increase in thermal energy available from HEX-2. This decreases the thermal energy demand in HEX-1. As described before, decreasing ΔT_{HEX-1} leads to decreased heat duty from HEX-2. Hence, both cases have lower fuel demand and thus higher product output, as less water is produced.

Fig. 16 shows the hydrogen efficiency for the different variable variations. Increasing T_{Burn}, X_{CO} and decreasing ΔT_{HEX-1}, H_2/CO, T_{FTS} leads to higher hydrogen efficiencies. As the hydrogen efficiency is directly related to the product output, the product output increases. The maximum hydrogen efficiency found in the base case, 725 °C and 1 bar, is confirmed for all variable variations.

In general, the carbon efficiency varies only marginally between 87

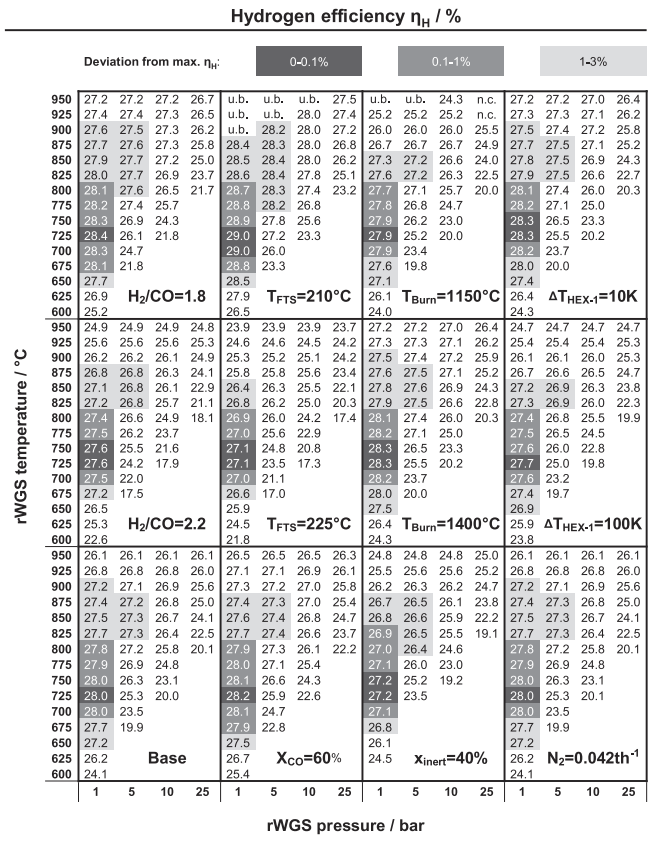

Fig. 16. Hydrogen efficiency for different assumptions, rWGS pressures and rWGS temperatures. N.c. – not converged: No value available for the given constellation. U.b. – upper boundary: Rec-rWGS approaches zero and the inert gas content exceeds the fixed 50 mol%.

and 90 %. It depends on the CO_2 recovery from the cement plant and purged gas. More purged gas decreases the carbon efficiency. The maximum carbon efficiency (90 %) is found for the variation of the impurities as the purged gas decreases with decreasing impurities. The influence of the rWGS operating conditions on the carbon efficiency is negligible (see chapter 3.3).

Comparison with literature results

To our knowledge, there is no experimental data available in the literature for the exact same configuration as described in this work. The closest resemblance of an experimental setup to the one described in this work can be found in [15]. The SOLETAIR pilot plant consists of a unit for direct air capture DAC, a PEM electrolyzer, a rWGS reactor with electrical heating and a FT micro-structured heat exchanger reactor [15]. In contrast to the configuration described in Chapter 2, there is no recycling of the gaseous FT products. The rWGS is operated at 850 °C and 4 bar and the operating conditions of the FT reactor are H_2/CO = 2.1, 230–240 °C and 20 bar [15]. No results are given for the PtL-efficiency. 30.8 % of the hydrogen and 59.5 % of carbon ends up in the FT product (including gaseous components) [15]. Applying the same operating conditions for the FTS (T_{FTS} is set to 230 °C) and rWGS in our process model gives a hydrogen efficiency of 27.3 %. The hydrogen efficiency in the pilot plant is probably slightly higher due to the fact that the heat for the rWGS is provided electrically and not by combustion of the recycling gas. The combustion of recycling gas increases water production, which decreases hydrogen efficiency. The carbon efficiency is higher in this work (η_C = 88 %) as the implementation of recycles increases the carbon efficiency, which was also observed in the analysis of a theoretical plant in [15]. In this theoretical plant a carbon efficiency of 94 % is calculated [15]. The carbon efficiency in [15] is based on the amount of CO_2 from the DAC, whereas in our definition it is based on the amount of CO_2 entering the MEA from the cement plant. Replacing the denominator in equation (xvi) by the amount of carbon recovered by the MEA unit, gives a carbon efficiency of 97%, which is slightly higher than the carbon efficiency in [15]. For the theoretical plant a PtL-efficiency of 47% (based on the higher heating value) is given in [15]. The maximum PtL-efficiency in this work is $\eta_{PtL,LHV}$ = 40.9 % (T_{FTS} = 210 °C, see Fig. 15), which equals $\eta_{PtL,HHV}$ = 44 % (based on the higher heating value HHV). The slightly lower PtL-efficiency is probably correlated to the slightly lower hydrogen efficiency. The hydrogen efficiency in the theoretical plant is 32 % which is close to the thermodynamic optimum of η_H = 33.3 % [15]. The highest hydrogen efficiency found in this work is 29 % (T_{FTS} = 210 °C, see Fig. 16). The slightly lower hydrogen efficiency is probably related to the difference in rWGS heat supply. In this work an allothermal rWGS reactor with oxyfuel burner is implemented, whereas the theoretical plant from [15] is equipped with an autothermal rWGS reactor. This possibly explains the difference in hydrogen efficiency, and further PtL-efficiency.

Conclusions

As neither the rWGS nor the FTS provide full conversion, recycles are necessary to increase the carbon efficiency of the PtL process. This increases the complexity of the process and thus, finding the optimum operating conditions for the rWGS unit within the FT-based Power-to-Liquid process is not straightforward. To find the optimum operating conditions in terms of energetic efficiency and H-/C-efficiency, a detailed process analysis was conducted. The findings of this process analysis can be summarized as follows:

- Increasing pressure and decreasing temperature in the rWGS reactor leads to increased methane formation. This affects the properties of the recycle and increases the recycle rates to the rWGS.
- For a given rWGS pressure there is a plateau, where the rWGS temperature has only minor influence on the efficiencies. Outside this plateau, the efficiencies decrease due to an increase in methane formation (low temperatures) and a decrease in HEX-1 efficiency (high temperatures).
- Intrinsically, the efficiencies are related to the product output. The product output correlates inversely with the water produced in the overall process. On the one hand, the water production correlates with the heating demand and the burner fuel composition, and hence, the recycle gas composition. Both are influenced mainly by the methane content in the rWGS product gas. On the other hand, the water production is influenced by the heat exchanger efficiency of HEX-1. The decrease in heat transfer at high temperatures (to avoid a temperature cross in the heat exchanger) leads to decreasing product output. The maximum product output is found at 725 °C and 1 bar.
- The H-efficiency correlates directly with the product output. Hence, the maximum efficiency (η_H = 28 %) is also found at 725 °C and 1 bar.
- The C-efficiency (η_C = 88 %) is not affected significantly by the rWGS operating conditions. It is restricted by the recovery rate of the MEA unit.
- The maximum Power-to-Liquid efficiency is obtained at 5 bar and 825 °C (η_{PtL} = 38.7 %). In comparison to the optimum operating conditions in terms of hydrogen efficiency, the energetic optimum is shifted towards higher rWGS pressure due to the decreased electricity required for compression. The optimum rWGS temperature is shifted towards higher temperature as higher temperatures are required to reach the same CO-selectivity (less methane formation).
- Pinch analysis shows a significant amount of excess high temperature heat available in the process. Using this high temperature heat to produce electricity may increase the overall PtL-efficiency. However, it has yet to be proven whether this is economically beneficial.

- Significant influence of the assumptions on the efficiencies is observed. However, the optimum rWGS operating conditions obtained in the base case are found to be in the highest PtL-efficiency ranges within the whole investigated parameter range (0.1% variation based on the respective $\eta_{PtL,max}$). This indicates robust rWGS optimum operating conditions.

Note: Although carbon formation is neglected in this work, it might narrow down the possible operating window of the rWGS, and thus, has to be further investigated in detail.

Declaration of Competing Interest

The authors declare that they have no known competing financial interests or personal relationships that could have appeared to influence the work reported in this paper.

References

[1] Paris Agreement. 2015, United Nations Framework Convention on Climate Change.
[2] Sims, R., et al., 2014: Transport, in Climate Change 2014: Mitigation of Climate Change. Contribution of Working Group III to the Fifth Assessment Report of the Intergovernmental Panel on Climate Change. 2014, Cambridge University Press: Cambridge, United Kingdom and New York, NY, USA. p. 606.
[3] Carbon offsetting for international aviation. 2019.
[4] Conference on aviation and alternative fuels. in Power-to-Liquids (PtL): Sustainable alternative fuels produced from renewable electricity. 2017. Mexico City.
[5] IATA Sustainable Aviation Fuel Roadmap. 2015(1).
[6] IATA, Resolution on the commercial deployment of sustainable alternative fuel for aviation. 2017: 73rd IATA Annual General Meeting.
[7] Steele, P., EU Renewable Energy Directive / Sustainable Aviation Fuel, in Open Letter from the IATA. 2018.
[8] Schmidt, P., et al., Power-to-Liquids as Renewable Fuel Option for Aviation: A Review. 2018. 90(1-2): p. 127-140.
[9] Becker, W., et al., Production of Fischer–Tropsch liquid fuels from high temperature solid oxide co-electrolysis units. 2012. 47(1): p. 99-115.
[10] Cinti, G., et al., Integration of Solid Oxide Electrolyzer and Fischer-Tropsch: A sustainable pathway for synthetic fuel. 2016. 162: p. 308-320.
[11] Fasihi, M., D. Bogdanov, and C. Breyer, Techno-economic assessment of power-to-liquids (PtL) fuels production and global trading based on hybrid PV-wind power plants. Energy Procedia, 2016. 99(10th International Renewable Energy Storage Conference, IRES 2016): p. 243-268.
[12] Herz, G., E. Reichelt, and M. Jahn, Techno-economic analysis of a co-electrolysis-based synthesis process for the production of hydrocarbons. 2018. 215: p. 309-320.
[13] König, D.H., et al., Simulation and evaluation of a process concept for the generation of synthetic fuel from CO2 and H2. 2015. 91: p. 833-841.
[14] Tremel, A., et al., Techno-economic analysis for the synthesis of liquid and gaseous fuels based on hydrogen production via electrolysis. 2015. 40(35): p. 11457-11464.
[15] Vázquez, F.V., et al., Power-to-X technology using renewable electricity and carbon dioxide from ambient air: SOLETAIR proof-of-concept and improved process concept. 2018. 28: p. 235-246.
[16] De Klerk, A., Fischer-tropsch refining. 2012: John Wiley & Sons.
[17] Rostrup-Nielsen, J. and L.J. Christiansen, Concepts in Syngas Manufacture, ed. W. S.P. Co.Pte.Ltd. Vol. Catalytic science series. 2011, Denmark: Imperial College Press, London.
[18] Finlayson, B.A., Introduction to chemical engineering computing. 2006: Wiley Online Library.
[19] Environmental Data of the German Cement industry. 2016: Duesseldorf.
[20] WindEnergie, B.B., Windenergie in Deutschland - Zahlen und Fakten. 2019.
[21] Estelmann, S., R.-U. Dietrich, and A. Seitz, Flexibilitätsoptionen in der Grundstoffindustrie Methodik| Potenziale| Hemmnisse. 2018.
[22] Schirrmeister, S. Power-to-X Anlagen im technischen Maßstab. in 2. Aachener Ofenbau- und Thermoprozess-Kolloquium. 2019. Aachen.
[23] Collins CD. Implementing phytoremediation of petroleum hydrocarbons. In: Phytoremediation. Springer; 2007. p. 99–108.
[24] Aftalion, F. and J.A. Kent, Handbook of industrial chemistry and biotechnology. 2012.
[25] von Schéele J. Technologies for energy and operation efficiency in stainless steel production. Linde India Limited 2015.
[26] Smolinka, T., M. Günther, and J. Garche, Stand und Entwicklungspotenzial der Wasserelektrolyse zur Herstellung von Wasserstoff aus regenerativen Energien: NOW-Studie: Kurzfassung des Abschlussberichts. 2011: Fraunhofer ISE.
[27] CO2 capture in the cement industry. 2008.
[28] Peters, M.S., et al., Plant design and economics for chemical engineers. Vol. 5. 2003: McGraw-Hill New York.
[29] S. Roussanaly et al. Techno-economic analysis of MEA CO2 capture from a cement kiln - impact of steam supply scenario 2017 Lausanne, Switzerland 14 18.
[30] Schmidt O, et al. Future cost and performance of water electrolysis: an expert elicitation study. Int J Hydrogen Energy 2017;42(52):30470–92.
[31] Bertuccioli, L., et al., Development of Water Electrolysis in the European Union. 2014, Fuel Cells and Hydrogen Joint Undertaking: Lausanne.
[32] Habermeyer, F., S. Adelung, and E. Kurkela, Flexible combined production of power, heat and transport fuels from renewable energy sources. Deliverable Report for EU Project FLEX CHX, 2018.
[33] Thema, M., F. Bauer, and M. Sterner, Power-to-Gas: Electrolysis and methanation status review. 2019. 112: p. 775-787.
[34] Wesenberg MH. Gas heated steam reformer modelling. Trondheim: Norwegian University of Science and Technology:; 2006. p. 11–2.
[35] Skogestad, S., Chemical and energy process engineering. 2008: CRC press.
[36] Sie ST, Senden MMG, Van Wechem HMH. Conversion of natural gas to transportation fuels via the shell middle distillate synthesis process. (SMDS) 1991;8 (3):371–94.
[37] Luque, R. and J. Clark, Handbook of biofuels production: Processes and technologies. 2010: Elsevier.
[38] Kaiser, P., F. Pöhlmann, and A. Jess, Intrinsic and Effective Kinetics of Cobalt-Catalyzed Fischer-Tropsch Synthesis in View of a Power-to-Liquid Process Based on Renewable Energy. 2014. 37(6): p. 964-972.
[39] Fratalocchi, L., et al., Intensifying heat transfer in Fischer-Tropsch tubular reactors through the adoption of conductive packed foams. 2018. 349: p. 829-837.
[40] Vervloet D, et al. Fischer-Tropsch reaction–diffusion in a cobalt catalyst particle: aspects of activity and selectivity for a variable chain growth probability. Catal Sci Technol 2012;2(6):1221–33.
[41] Kaiser, P., et al., Production of liquid hydrocarbons with CO2 as carbon source based on reverse water-gas shift and Fischer-Tropsch synthesis. 2013. 85(4): p. 489-499.
[42] Kaiser, P. and A. Jess, Modeling of multitubular reactors for Iron-and Cobalt-catalyzed Fischer–Tropsch syntheses for application in a power-to-liquid process. 2014. 2(5): p. 486-497.
[43] Leckel, D. and M. Liwanga-Ehumbu, Diesel-selective hydrocracking of an iron-based Fischer– Tropsch wax fraction (C15– C45) using a MoO3-modified noble metal catalyst. 2006. 20(6): p. 2330-2336.
[44] Coonradt HL, et al. Mechanism of hydrocracking. Reactions of Paraffins and Olefins. 1964;3(1):38–45.
[45] Adelung, S., D. Schnellbögl, and R.-U. Dietrich, Reaktionskinetik der reversen Wassergas-Shift Reaktion bei Normaldruck zur Übertragung auf die Synthesegasbereitstellung im PtL-Prozess.
[46] Albrecht, F.G., et al., A standardized methodology for the techno-economic evaluation of alternative fuels–A case study. 2017. 194: p. 511-526.
[47] Visconti, C.G. and M. Mascellaro, Calculating the product yields and the vapor–liquid equilibrium in the low-temperature Fischer–Tropsch synthesis. 2013. 214: p. 61-73.
[48] Yang, J., et al., Fischer–Tropsch synthesis: A review of the effect of CO conversion on methane selectivity. 2014. 470: p. 250-260.